DRAFT VERSION AUGUST 11, 2019
Typeset using LaTeX **twocolumn** style in AASTeX62

Helium Stars as Progenitors of Thermonuclear Supernovae: Dependence on Metallicity and Overshooting

S. CHANLARIDIS,[1] J. ANTONIADIS,[1,2] G. GRÄFENER,[1] AND N. LANGER[1,2]

[1]*Argelander-Institut für Astronomie, University of Bonn, Auf dem Hügel 71, D-53121 Bonn, Germany*
[2]*Max-Planck-Institut für Radioastronomie, Auf dem Hügel 69, D-53121 Bonn, Germany*

(Received XXX; Revised YYY; Accepted ZZZ)

Submitted to AAS

ABSTRACT

Type Ia supernovae (SNe Ia) are luminous optical transients characterized by the absence of hydrogen and helium in their spectra. The majority of SNe Ia are thought to result from the thermonuclear disruption of white dwarfs, which is triggered by mass accretion in a binary system. However, both the details of the explosion mechanism and the exact nature of the progenitor systems remain a topic of debate. Recent results from wide-field transient surveys, suggest that SNe Ia are far more diverse than previously thought. This diversity could be the result of varied progenitor systems. We have discovered a novel SN Ia progenitor channel, in which a thermonuclear explosion is initiated during the late evolution of stripped helium stars with masses between $\sim 1.8-2.7\,M_\odot$ which are frequently produced from the mass donors in interacting massive, close binaries. This mechanism does not require accretion from the binary companion and therefore may contribute significantly to the SN Ia rate in star-forming galaxies (i.e. at early delay times).

Keywords: stars: evolution — white dwarfs — supernova: general — nuclear reactions, nucleosynthesis

1. INTRODUCTION

Helium stars (He stars) are the exposed, naked cores of hydrogen deficient stars that have lost their hydrogen-rich mantle either via stellar winds or mass transfer episodes, if it happens to be part of a binary system. For progenitor stars in the initial mass range $M_i \approx 8-10\,M_\odot$, carbon will be ignited in a shell, following the depletion of helium supply in their cores. Responsible for this off-centre ignition is significant neutrino cooling that occurs deep in the stellar core, and shifts the location of maximum temperature (temperature inversion) to the aforementioned shell. This marks the transition of the star toward the super-asymptotic giant branch (SAGB). The heat generated from the burning shell creates a subsonic carbon-burning front ("C-flame") that propagates inward. The physical properties of such a deflagration have been the subject of various studies (e.g. Timmes et al. 1994; Siess 2006, 2009; Denissenkov et al. 2013; Farmer et al. 2015) and show a strong dependency on the adopted initial parameters.

As this C-flame moves toward the centre, it will process the material of the partially degenerate carbon-oxygen (CO) core converting it into an oxygen-neon (ONe) core. The subsequent evolution that will determine the final fate of the star, depends on the interplay between the core mass growth rate and the mass loss rate. If shell burning allows the core to reach the critical mass value of $\sim 1.37\,M_\odot$ (Nomoto 1984), the central density becomes sufficiently high ($\rho_c \sim 10^{9.95}$ gr cm^{-3}) for electron captures on ^{24}Mg and ^{20}Ne nuclei to ensue, essentially reducing the pressure in the interior, and ultimately leading to the collapse of the core; this is referred to as *electron capture supernova* (ECSN). The end product of an electron capture induced collapse would be a low-mass neutron star formed from a dim supernova (e.g. Fischer et al. 2010, and references therein) with relatively low explosion energy, which imparts only a small natal kick to the remnant (Knigge et al. 2011; Jones et al. 2013; Jones et al. 2016) compared to the iron core collapse (Fe-CCSN) channel.

On the other hand, if the central density does not reach the threshold for electron captures on the most abundant species, the star will shed its envelope before the core reaches the Chandrasekhar mass limit (M_{ch}), and end up as an ONe white dwarf (ONe WD). However, if the ONe WD is in a close binary system, it can evolve to a supernova following a similar path as the one described above. This can be realized with the transfer of mass from the companion star onto the surface of the WD, allowing it to grow near the Chandrasekhar mass and leave behind a neutron star, a scenario that is known as *accretion-induced collapse* (AIC) (e.g. Nomoto & Kondo 1991; Schwab et al. 2015; Brooks et al. 2017; Schwab & Rocha 2019).

Corresponding author: Savvas Chanlaridis
schanlar@astro.uni-bonn.de

1.1. *Thermonuclear Supernovae*

Due to lack of a hydrogen envelope, the collapsing core of a He star would be observed as a type Ib/c supernova, depending on the degree of stripping as has been shown by Tauris et al. (2013, 2015). In the case of normal SAGB stars that retain a hydrogen-rich mantle, the spectral lines could resemble the ones found in types IIn-P supernovae (see Moriya et al. 2014, for details).

Nonetheless, one should keep in mind that by the time the effects of electron captures on nuclei cannot be neglected, the necessary pressure gradient against gravity is provided by a strongly degenerate electron gas. For degenerate matter, pressure does not depend on the temperature thus the star can no longer respond to a temperature increase by expanding its outer layers. Since thermonuclear reaction rates are extremely sensitive to temperature variations, under such degenerate conditions, even a small increase of temperature caused by ignition of the existing nuclear fuel, could alter the nuclear burning rate dramatically resulting in a thermal runaway.

Whether the ONe WD undergoes core collapse or experiences a thermonuclear explosion depends on the timescale of electron captures versus the timescale of nuclear energy release. Since electron captures become energetically favorable only above specific values of central density, the ignition location of explosive nuclear burning plays a major role to the final result. Indeed, Jones et al. (2016) have demonstrated that for low ignition density, the core does not collapse into a neutron star but rather explodes leaving behind bound remnants.

The consideration above is consistent with the explosion mechanisms (e.g. single degenerate model) related to type Ia supernovae (for recent reviews see Hillebrandt & Niemeyer 2000; Wang & Han 2012; Wang 2018; Livio & Mazzali 2018). It becomes apparent that ECSNe could originate from a variety of progenitor systems either in single or binary configuration, and the connection between the progenitor and the final outcome is far from trivial.

1.2. *The Urca process*

The term "Urca-processes" was introduced by Gamow & Schoenberg (1941) in order to describe energy losses from neutrino emission. It consists of two weak nuclear reactions: an electron capture that operates on a mother nucleus $M \equiv (A, Z)$ forming a more neutron-rich, daughter isobar $D \equiv (A, Z-1)$

$$(A, Z) + e^- \longrightarrow (A, Z-1) + \nu_e \tag{1}$$

and a beta-decay transition of D back to M

$$(A, Z-1) \longrightarrow (A, Z) + e^- + \bar{\nu}_e \tag{2}$$

where A and Z denote respectively the mass number and the atomic number of the nucleus. The mother-daughter pair $({}^{A}_{Z}M, {}^{A}_{Z-1}D)$ can be referred to as "Urca nuclei".

As central density increases, the Fermi energy ϵ_F (or equivalently the electron chemical potential, μ_e) of the relativistic, degenerate Fermi gas prevails over the threshold energy E_t of a given Urca nuclei pair (i.e. the difference between the rest masses of M and D, given by the Q value for a ground state to ground state transition), and electron captures will commence promptly. The associated reaction rates (λ^+, λ^-), and neutrino energy losses (L^+, L^-) per nucleon for equations 1, 2 respectively, have been calculated by Tsuruta & Cameron (1970) and exhibit a strong sensitivity on temperature and density. Therefore, Urca processes become important only for a narrow range of stellar plasma properties, defining a thin Urca shell in which they operate (where $\epsilon_F = E_t$).

Paczyński (1972) argued that during the simmering phase of a CO WD, the energy released from carbon burning would not be able to be transferred efficiently via radiative means leading to a convective core that could engulf the Urca shell (convective Urca). Ultimately, the Urca neutrinos[1] would carry away enough energy to delay the dynamical runaway and forcing the core to move to higher densities thus, collapsing into a neutron star. However, Bruenn (1973) challenged this notion by showing that Urca processes can also have destabilizing effects by generating heat, if convective motions re-position the relevant nuclei at some distance from the Urca shell. In these non-equilibrative states, if e-capture dominates over the β-decay (i.e. if $\rho > \rho_{\rm th}$), the captured electron creates a "hole" in the Fermi sea and forces another electron to drop from the Fermi surface in order to fill the gap, resulting in heating. On the other hand, if $\rho < \rho_{\rm th}$, β-decay liberates electrons with excess thermal energy that also results in heating. Therefore, convective Urca processes can either play a major role as local cooling mechanisms (at mass coordinate in the vicinity of the Urca shell where both reactions are in equilibrium) or contribute to heating outside the Urca shell.

The effect of convective Urca processes on stellar interiors remain still an open question and provides up to this day fertile ground for debate. For a more detailed analysis, and fruitful discussion on the physics and importance of Urca process we refer to the work of Paczyński (1973); Barkat & Wheeler (1990); Stein et al. (1999); Lesaffre et al. (2005); Waldman & Barkat (2007); Denissenkov et al. (2015); Schwab et al. (2017).

The structure of this paper is organized as follows. In Section 2, we present the input physics we used to model the evolution of our He-stars. In Section 3, we discuss our results and their implications to our current state of knowledge. Section 4 provides a summary of our results and necessary future work.

[1] Here we use the term "neutrinos" to refer both to neutrinos and antineutrinos interchangeably.

2. STELLAR EVOLUTION CODE AND INITIAL PARAMETER SPACE

We performed numerical calculations using the one dimensional, stellar evolution code **M**odules for **E**xperiments in **S**tellar **A**strophysics (MESA), version - r10398 (Paxton et al. 2011, 2013, 2015, 2018, 2019).

2.1. *Physical assumptions*

Our grid consists of 252 single He stars in the mass range $0.8 \leq M/M_{\odot} \leq 3.5$ with a step of 0.1. Evolutionary calculations begin from the pre-main sequence phase with a uniform initial composition. In order to study the effects of metallicity, we create a series of models with low ($Z = 0.0001$), intermediate ($Z = 0.001$), and solar metallicity ($Z \equiv Z_{\odot} = 0.02$). Similarly, for varying the efficiency of overshooting we create series with no overshooting ($f_{\rm ov} = 0.0$), and overshoot mixing ($f_{\rm ov} = 0.014$, $f_{\rm ov} = 0.016$) across all convective boundaries. The free parameter $f_{\rm ov}$ is defined in Herwig (2000) as a fraction of the local pressure scale height, H_p, and is connected to the diffusion coefficient, $D_{\rm OV}$, via the relation given by equation 3, where z is the geometric distance from the edge of the convective zone.

$$D_{\rm OV} = D_0 \exp\left(-\frac{2z}{H_v}\right), \qquad H_v = f_{\rm ov} \cdot H_p \tag{3}$$

The choice of an adequate nuclear network and accurate weak rates are aspects of paramount importance in our considered mass-range, since we expect substantial amounts of ^{23}Na, ^{25}Mg, and ^{27}Al to be produced after the carbon burning phase. Urca process operating on those odd-mass-number nuclei can alter the energy balance with a significant impact upon the thermal structure of the core. For this reason, we construct a nuclear reactions network that consists of forty-three nuclear species, including important NeNa and MgAl cycles, and relevant weak reactions for several Urca pair isotopes. Finally, we incorporate the special weak rates from Suzuki et al. (2016).

We considered ion and electron screening corrections as described in Potekhin et al. (2009) and Itoh et al. (2002) respectively. To account for an enhanced carbon-oxygen mixture as a result of helium burning, we used the Type-2 OPAL Rosseland mean opacity tables (Iglesias & Rogers 1996). For the equation of state blending we followed the options suggested by Schwab et al. (2017).

Convection was treated according to the standard mixing-length theory prescription of Henyey et al. (1965) with a mixing-length parameter of $\alpha_{\rm ML} = 2.0$. Furthermore, we used the Ledoux criterion for convective instability adopting an efficiency parameter of $\alpha_{\rm SEM} = 1.0$ for semi-convection (Langer 1991), and a diffusion coefficient $D_{\rm TH} = 1.0$ for thermohaline mixing (Brown et al. 2013). Both semi-convection and thermohaline mixing are treated by MESA as diffusive processes (Langer et al. 1983; Kippenhahn et al. 1980).

Table 1. Baseline parameters for single helium stars

Parameter	Value(s)
Convection ($\alpha_{\rm ML}$)	2.0
Semiconvection ($\alpha_{\rm SC}$)	1.0
Thermohaline ($D_{\rm TH}$)	1.0
Wind scaling factor (η)	1.0
Overshooting ($f_{\rm ov}$)	0.0, 0.014, 0.016
Metallicity (Z)	10^{-4}, 10^{-3}, 0.02

Mass loss rates due to stellar winds were implemented using the "`Dutch`" wind scheme (Glebbeek et al. 2009). In our case, this implies two different rates depending on the effective temperature of the star; for $T_{\rm eff} > 10^4$ K and a surface abundance of hydrogen $X < 0.4$ by mass fraction (which is always satisfied for the models we developed), we apply the prescription of Nugis & Lamers (2000) with a scaling factor of $\eta = 1$ (canonical value). For $T_{\rm eff} < 10^4$ K the mass loss rate follows the prescription of de Jager et al. (1988).

All the baseline parameters we adopted above are summarized in Table 1, and the MESA inlists will become publicly available[2].

3. RESULTS

3.1. *Overview of the Evolution*

As it was mentioned in section 2.1, we followed the evolution of He-stars in the mass range $0.8 - 3.5$ M$_{\odot}$ starting from the pre-main sequence phase with a uniform initial composition. After the end of core helium burning, the mass fraction of carbon in the newly formed metal core is within the range $0.31 \lesssim X_C \lesssim 0.48$. Since the abundances of other species can be neglected in this stage, the mass fraction of oxygen can be taken as the complement to unity with respect the aforementioned carbon mass fraction range.

Following the depletion of helium in the core, a radiative helium-burning shell is being formed that forces the core to grow in mass. From this point, we can distinguish four different evolutionary paths; if the core mass (M$_c$) is below a lower limit M$_{\rm low}$ that depends on the adopted values for metallicity and overshooting, then carbon is never ignited and the star will end up as a carbon-oxygen white dwarf.

In the case of $\mathrm{M_{low}} \leq \mathrm{M_c} < \mathrm{M_{up}^{hyb}}$, where $\mathrm{M_{up}^{hyb}}$ is an arbitrary upper limit, carbon is ignited off-centre while the core expands and cools as a result of shell-burning. The C-flame advances inward in a series of flashes, but fails to reach the centre. The ignition location depends on both the initial mass of the star, and the carbon mass fraction. The flame quenching can be attributed to several physical mechanisms, e.g. overshoot mixing (Denissenkov et al. 2013; Chen et al. 2014;

[2] http://cococubed.asu.edu/mesa_market/inlists.html

Farmer et al. 2015), and thermohaline mixing (Siess 2009). The star in this case, will end up as a hybrid CONe white dwarf. Nevertheless, Lecoanet et al. (2016) have shown that buoyancy prevents convective plumes to penetrate into the flame since they are not dense enough, hence convective mixing is insufficient to stall a carbon flame making such hybrid WDs a non-typical product of stellar evolution.

If $M_{up}^{hyb} \leq M_c < M_{up}$, where M_{up} is once again an arbitrary upper limit, the C-flame is able to propagate all the way toward the center, forming an ONe core. However, our simulations show that in all cases, carbon is not being burned up completely, and an amount of $0.003 \lesssim X_C \lesssim 0.23$ by mass fraction is still present and distributed throughout the core. The presence of carbon may lead to explosive burning as has been suggested by (Schwab & Rocha 2019; Waldman & Barkat 2007, hereafter SR19, and WB07 respectively) and Gutiérrez, J. et al. (2005). However, both of these works investigate the effect of residual carbon in a binary system, where carbon is ignited only after a cooled-down WD, with a "frozen" carbon profile has reached the Chandrasekhar limit via accretion (AIC). The ignition density of the runaway may vary with the amount of left-over carbon, resulting in a fairly wide range of ejecta velocities and compositons. In this work, we demonstrate that the Chandrasekhar limit may be achieved via shell burning, without the need of an extended accretion phase. The runaway ignition location does not show any significant variability among our models. This is perhaps due to the nature of the degenerate cores, which are still very hot in contrast to the ONe WDs of SR19 and WB07 that have achieved homogenization via thermocompositional mixing. Additionally, the stabilizing temperature gradient in our models prohibits thermohaline mixing to re-distribute and destroy the gradient of the residual carbon profile in the core. More importantly, it prevents the destruction of the stratified core-mantle structure in hybrid CONeMg cores that would occur as the WD cools down, allowing them to grow to near Chandrasekhar masses (see also Brooks et al. 2017; Schwab & Garaud 2019).

Finally, if $M_c \geqslant M_{up}$ then carbon is ignited on-centre leading to more advanced burning stages, and ultimately the star undergoes core collapse whilst a neutron star is formed.

3.2. *Core Growth and Structure*

In the next sections, we are going to discuss the growth of hybrid and oxygen-neon cores and how their structure is affected by the metallicity environment and overshoot mixing, without concerning ourselves with the extreme cases of white dwarfs, or core collapsing stellar models.

Following the off-centre carbon burning phase, the core of the star is either dominated by carbon and oxygen which is engulfed in an ONeMg shell, or -if the C-flame reaches the centre- the degenerate core is composed primarily of oxygen and neon, with a small amount of carbon that remains unburned. In the latter case, we choose a fiducial model of 2.5 $M_\odot$, with solar metallicity and no overshooting, as representative of similar structured models, in order to demonstrate their evolution. The centre contracts and heats up whilst the

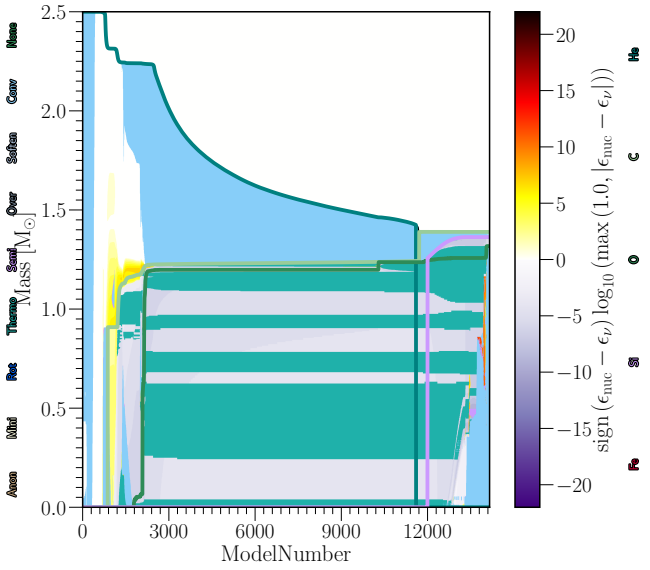

Figure 1. Kippenhahn diagram of the $2.5M_\odot$ helium star with $Z = 0.02$ and no overshooting that leads to the final structure shown in Figure 5(c). Blue areas denote regions with convection; green-coloured areas indicate thermohaline mixing. The intensity shown in the colour-bar, indicates the net energy-production rate. During the carbon simmering phase the core becomes convective.

envelope expands and develops a deep convective region that penetrates into the helium-burning shell as can be seen in Figure 1. The plot shows a cross-section of the helium star in mass coordinates along the y-axis, starting from the center and moving towards the surface of the star, as a function of stellar model number.

The core of our stellar models in the mass range $M_i = 1.8 - 2.7$ $M_\odot$ grow to near Chandrasekhar masses due to helium shell-burning, and reach a plateau of $M_c \sim 1.36 \pm 0.01$ $M_\odot$ whilst the extended He-rich envelope is easily ejected via a strong wind (see section 3.3 for discussion). Subsequently, the existing carbon in the core ignites initiating convective motions that feed the core with more carbon, and the star enters a carbon simmering phase. The energy yield from carbon burning is sufficient to raise the temperature for explosive oxygen burning under extreme degenerate conditions to occur. As a result, a thermal runaway ensues and the star which contains no helium at the time of the explosion, it would be observable as a SN Ia.

Convective overshooting leads to larger convective cores which, naturally, prolongs the time the star spends in the helium main-sequence phase and thus, lengthens its total lifetime. The reason is that an enlarged convective zone will supply the helium burning core with more fuel. The additional fuel will affect the rate at which nuclear energy is released, thus we expect higher luminosity in the cases where convective overshoot mixing is included. Moreover, the increased size of the metal core will shift the mass range for which we observe the behaviour described above, to lower initial masses. This shifting in the initial mass range caused

by the overshoot mixing and the metallicity is more evident and easily understood in Figure 3 where we display the full parameter space.

On the other hand, metallicity seems to adversely affect core growth. The effects of overshooting and metallicity on core growth can be seen in Figure 2 which shows the final core mass of our stellar models as a function of the initial mass. Missing data points correspond to models for which the code crashed before they were able to get rid of their helium envelope, thus we couldn't follow the evolution past the hot bottom burning phase and obtain a reliable estimate for the final core mass. The scattering that appears at the high-end of our grid is most likely due to the fact that these models stopped at different evolutionary stages; nonetheless, in all of those cases, the core mass has either exceeded the Chandrasekhar mass limit, or the star has developed an ONeSi structure that will eventually lead to a core-collapse, rendering these models irrelevant to our work.

Figure 3 illustrates our parameter space in a raster format. The color of each pixel indicates the composition of the star at the time the evolution was terminated. Since all models with an ONe structure (green pixels) grow to near Chandrasekhar masses, they will undergo thermal runaway as a result of the remaining carbon in their cores, avoiding this way to end up as oxygen-neon white dwarfs.

3.3. *Wind and Ejection of Inflated Envelopes*

[Gräfener]

3.4. *The Role of Residual Carbon*

3.4.1. *Oxygen-Neon Cores*

As the core is compressed, its density keeps on rising until it reaches the threshold of various Urca pairs. The ^{25}Mg - ^{25}Na, and ^{23}Na - ^{23}Ne pairs are of utmost importance in our case, and occur at densities $\log(\rho_c) \approx 9.1$, and $\log(\rho_c) \approx 9.2$ respectively. Tsuruta & Cameron (1970) have shown that the energy loss rate via Urca-cooling depends on the fourth power of temperature ($\propto T^4$), hence this effect is more prominent in our hot, young ONe cores rather than in cooled WDs.

The effect of Urca-cooling can be seen in Figure 4 where the evolution of our fiducial stellar model with initial mass of $2.5\mathrm{M}_\odot$, and solar metallicity is being displayed (blue line). The density at which carbon is ignited is illustrated with a dotted black line, taken from MESA; however, MESA assumes a 100% composition of carbon and thus, the limits shown in Figure 4 are only approximated. In our models, Urca-cooling occurs before central density reaches the threshold for carbon ignition, effectively shifting the simmering phase to higher densities, delaying the ignition of carbon, and altering the nucleosynthetic signature of the explosion.

Further compression leads to exothermic e-captures on ^{24}Mg nuclei. The generated heat ignites the residual carbon in a very localized manner due to the sensitivity of carbon reaction rates to temperature. This can be seen as a saw-tooth feature in Figure 4, where heating from carbon simmering antagonizes neutrino cooling. We did not investigate the effect of ^{24}Mg mass fraction, however Gutiérrez, J. et al. (2005) have shown that it could play a major role on the subsequent evolution.

The energy yield from carbon burning will eventually lead to dynamical burning of oxygen. Woosley et al. (2004) estimates that the end of the carbon simmering phase occurs roughly at $\log(T_c/\mathrm{K}) \approx 8.9$.

In order to mimic a carbon-free core and demonstrate the effects of residual carbon, we evolve a series of models for which we have set the rate of all carbon-consuming nuclear reactions to zero, once they reached a central density of $\log(\rho_c) = 9.0$ for the first time (grey circle in Figure 4). In this case, the compression continues achieving a balance between neutrino cooling and compressional heating. The core density continues to grow until it surpasses the threshold for e-captures on ^{20}Ne nuclei which leads to the ignition of oxygen burning. The competition between the propagating oxygen deflagration and e-captures on the post-deflagration NSE material will determine the final fate of the star. Recently, Zha et al. (2019) found that the deflagration starting from $\log(\rho_c/\mathrm{g\ cm^{-3}}) > 10.01$ leads to a collapse, reinforcing our notion that a carbon-free ONe core will, most likely, evolve towards an ECSN and ultimately in the formation of a low-mass neutron star.

3.4.2. *Hybrid CONeMg Cores*

A small number of models develop a hybrid CO/ONe structure in their core, but still reach the Chandrasekhar limit. We choose a fiducial model of $1.8\mathrm{M}_\odot$, with solar metallicity and overshooting ($f_{\mathrm{OV}} = 0.014$), in order to demonstrate the evolution of similar structured models.

Since the C-flame does not reach the centre, the Urca pairs ^{25}Mg - ^{25}Na, and ^{23}Na - ^{23}Ne, which are byproducts of carbon burning, are not in abundance. Thus, Urca cooling does not play any major role in the evolution of hybrid cores. In the absence of the aforementioned Urca pairs, the compression of the core will continue until the ignition of carbon, and explosive oxygen burning at lower densities compared to the case of of non-hybrid stellar models, leading to more energetic explosions (magenta line in Figure 4).

The structure of such hybrid proto-WDs is susceptible to mixing due to their composition gradient. As Brooks et al. (2017) point out, the ONe mantle has been processed by a carbon burning front that involves several weak reactions, resulting in a lower electron-to-baryon fraction (Y_e) with respect to the CO core. This configuration is stable against convection as long as the ONe ashes in the top, heavy fluid (mantle) are much hotter than the CO bottom, light fluid (core). As the temperature gradient is reduced, the core-mantle interface will be subjected to thermocompositional convection and destroyed in a timescale of the order of Kyr, as the WD moves toward an isothermal profile. By the time an explosion can occur, the WD should be well mixed. The same process can re-distribute the residual carbon within ONe cores and reduce it to such levels so a thermal runaway would be unlikely making the AIC a more plausible scenario.

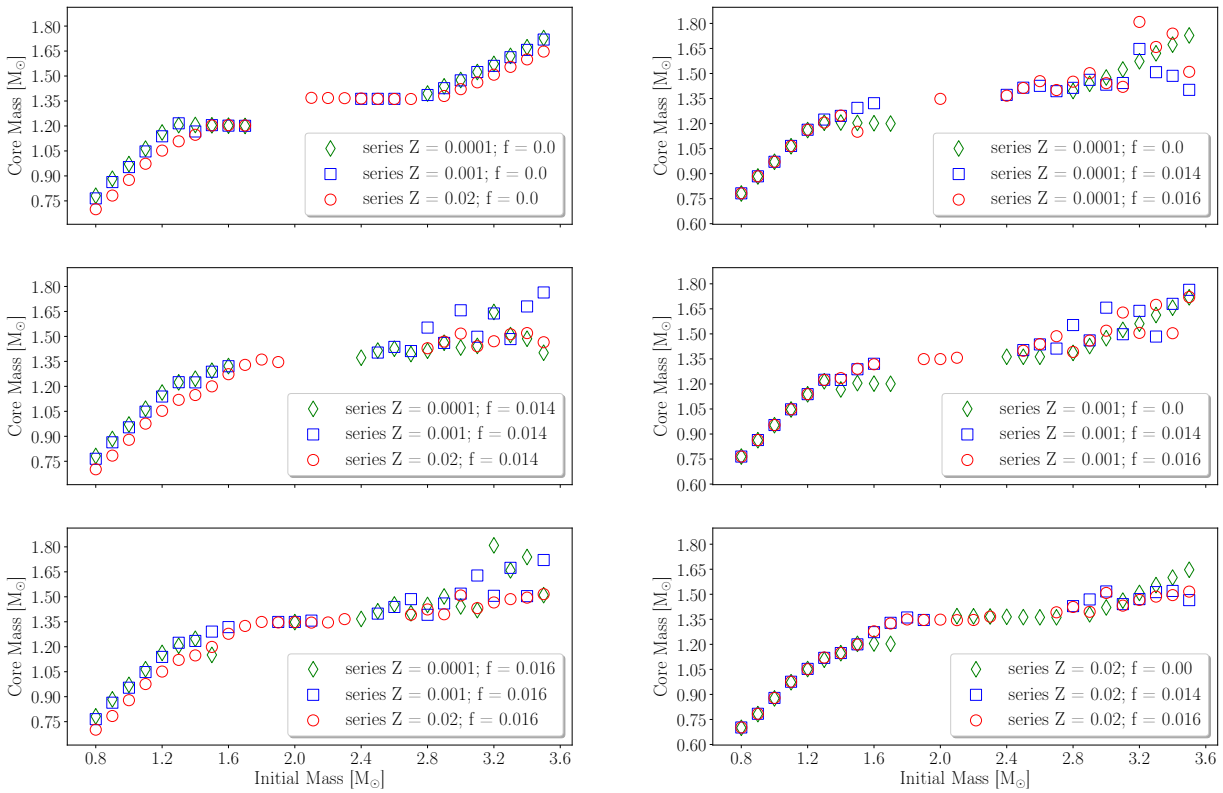

Figure 2. Core growth for different metallicity environments (left), and overshooting factors (right). Models that experience thermal runaway develop a core of $M_c \sim 1.36 \pm 0.01$ M$_\odot$ (plateau) due to He-shell burning. Missing data points correspond to models which their evolution ended abruptly, hence their final core mass could not be estimated.

3.5. *Observational Consequences*

[Antoniadis]

4. DISCUSSION AND FUTURE WORK

5. ACKNOWLEDGEMENTS

Software: MESA[3] (Paxton et al. 2011, 2013, 2015, 2018, 2019), ASTROPY[4] (Astropy Collaboration et al. 2013, 2018), MESAPLOT[5] (Farmer 2018), MESAREADER[6]

[3] http://mesastar.org
[4] http://www.astropy.org
[5] https://github.com/rjfarmer/mesaplot
[6] http://wmwolf.github.io/MESA_Reader

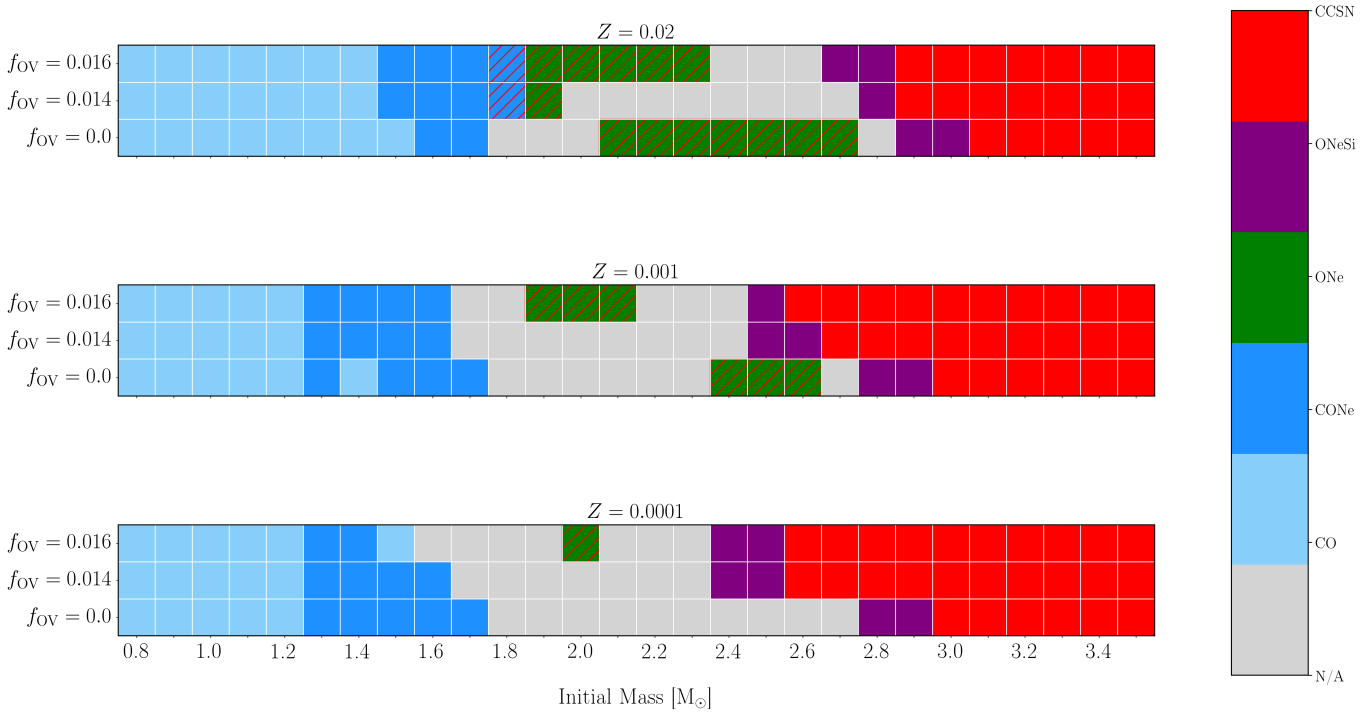

Figure 3. Full parameter space in raster format. Metallicity for the bottom, middle, and top panel is $Z = 0.0001$, $Z = 0.001$, and $Z = 0.02$ respectively, whilst the color-bar indicates the composition of the model at the moment our simulation was terminated. Hatched regions show models that have developed a core mass in the range 1.35 - 1.37 $M_\odot$, and can experience a thermonuclear runaway.

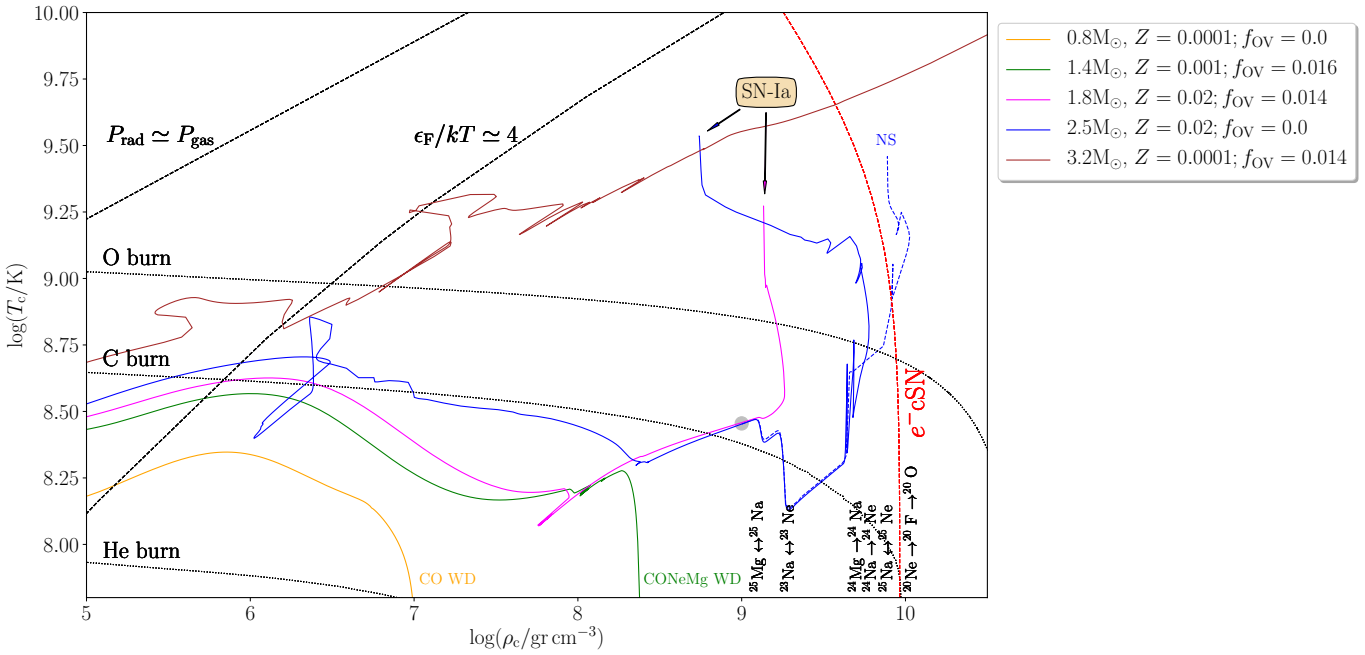

Figure 4. Examples of the evolution of different initial masses in the $\log(\rho_{\rm c}) - \log(T_{\rm c})$ plane. Black dotted lines show approximate ignition curves taken from MESA. Black dashed lines indicate different pressure regimes whilst the red dashed curve shows the approximate threshold for e-captures on ^{20}Ne nuclei. The blue dashed line refers to the same stellar model as the one with the solid blue line; the only difference is that for the former, all carbon-participating reaction have been switched off leading most likely to an ECSN.

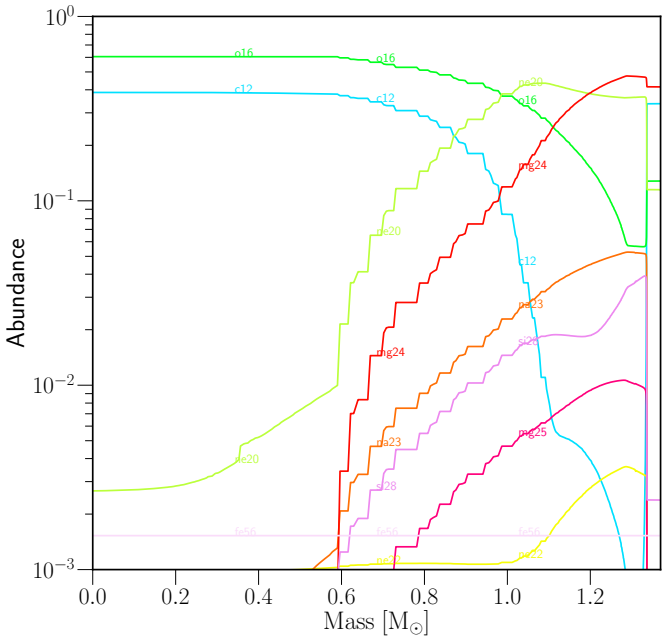

(a) Structure of the $1.8 M_\odot$, Z = 0.02; $f_{OV} = 0.014$ stellar model, when $\log(\rho_c) = 9.0$ (indicated by the grey circle in Figure 4).

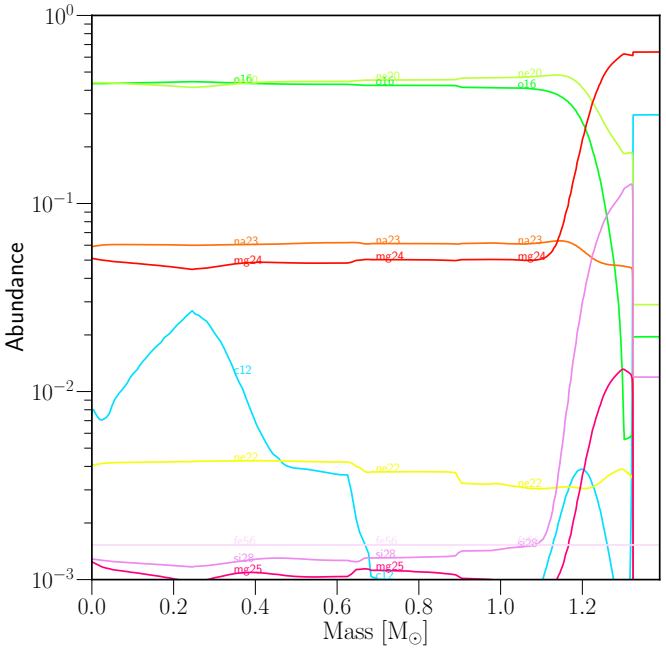

(b) Structure of the $2.5 M_\odot$, Z = 0.02; $f_{OV} = 0.0$ stellar model, when $\log(\rho_c) = 9.0$ (indicated by the grey circle in Figure 4). Residual carbon from previous burning stages is visible.

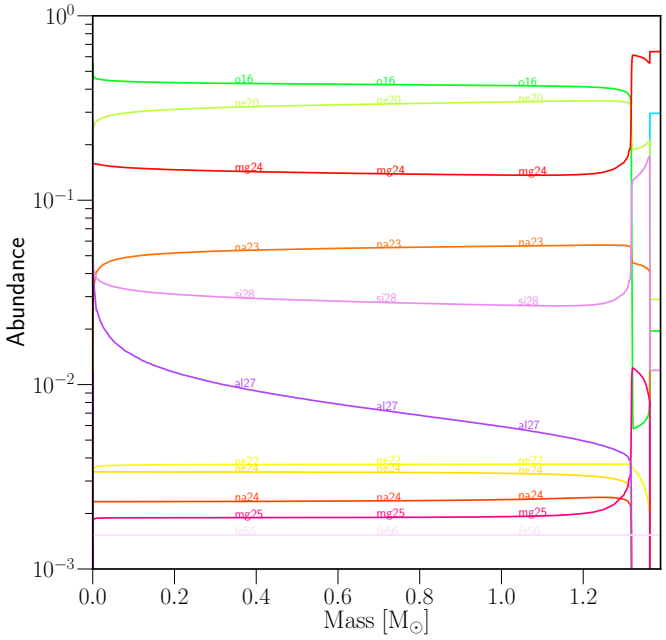

(c) Final structure of the $2.5 M_\odot$ stellar model. Residual carbon leads to TNE.

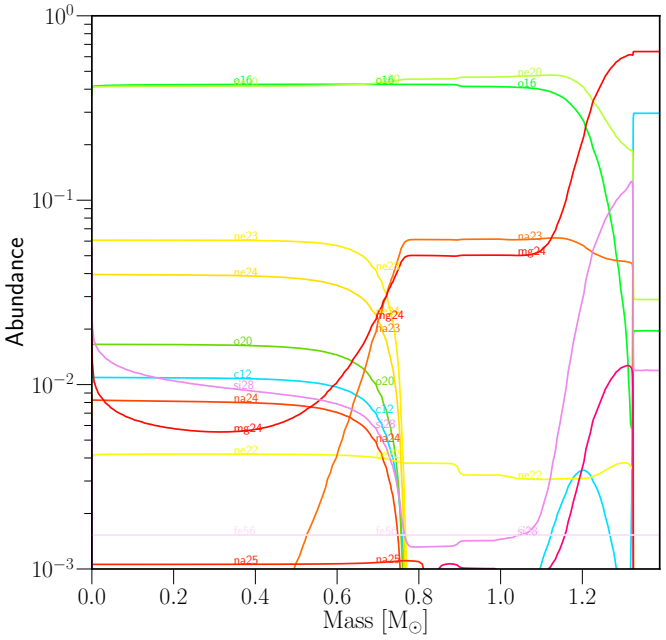

(d) Final structure of the $2.5 M_\odot$ stellar model, in the case where carbon consuming nuclear reactions have been turned-off. The core reach density for Urca process on Ne nuclei to commence, leading to formation of ^{20}O, and ultimately to ECSN.

Figure 5. Abundance profiles of our fiducial models during various evolutionary stages.

REFERENCES

Astropy Collaboration, Robitaille, T. P., Tollerud, E. J., et al. 2013, A&A, 558, A33

Astropy Collaboration, Price-Whelan, A. M., Sipőcz, B. M., et al. 2018, The Astronomical Journal, 156, 123

Barkat, Z., & Wheeler, J. C. 1990, ApJ, 355, 602

Brooks, J., Schwab, J., Bildsten, L., Quataert, E., & Paxton, B. 2017, The Astrophysical Journal, 843, 151

Brooks, J., Schwab, J., Bildsten, L., Quataert, E., & Paxton, B. 2017, ApJL, 834, L9

Brown, J. M., Garaud, P., & Stellmach, S. 2013, The Astrophysical Journal, 768, 34

Bruenn, S. W. 1973, ApJL, 183, L125

Chen, M. C., Herwig, F., Denissenkov, P. A., & Paxton, B. 2014, MNRAS, 440, 1274

de Jager, C., Nieuwenhuijzen, H., & van der Hucht, K. A. 1988, Astronomy and Astrophysics Supplement Series, 72, 259

Denissenkov, P. A., Herwig, F., Truran, J. W., & Paxton, B. 2013, The Astrophysical Journal, 772, 37

Denissenkov, P. A., Truran, J. W., Herwig, F., et al. 2015, MNRAS, 447, 2696

Farmer, R. 2018, rjfarmer/mesaplot

Farmer, R., Fields, C. E., & Timmes, F. X. 2015, The Astrophysical Journal, 807, 184

Fischer, T., Whitehouse, S. C., Mezzacappa, A., Thielemann, F. K., & Liebendörfer, M. 2010, A&A, 517, A80

Gamow, G., & Schoenberg, M. 1941, Phys. Rev., 59, 539

Glebbeek, E., Gaburov, E., de Mink, S. E., Pols, O. R., & Portegies Zwart, S. F. 2009, Astronomy and Astrophysics, 497, 255

Gutiérrez, J., Canal, R., & García-Berro, E. 2005, A&A, 435, 231

Henyey, L., Vardya, M. S., & Bodenheimer, P. 1965, The Astrophysical Journal, 142, 841

Herwig, F. 2000, Astronomy and Astrophysics, 360, 952

Hillebrandt, W., & Niemeyer, J. C. 2000, Annual Review of Astronomy and Astrophysics, 38, 191

Iglesias, C. A., & Rogers, F. J. 1996, The Astrophysical Journal, 464, 943

Itoh, N., Tomizawa, N., Tamamura, M., Wanajo, S., & Nozawa, S. 2002, The Astrophysical Journal, 579, 380

Jones, S., Röpke, F. K., Pakmor, R., et al. 2016, A&A, 593, A72

Jones, S., Hirschi, R., Nomoto, K., et al. 2013, The Astrophysical Journal, 772, 150

Kippenhahn, R., Ruschenplatt, G., & Thomas, H.-C. 1980, Astronomy and Astrophysics, 91, 175

Knigge, C., Coe, M. J., & Podsiadlowski, P. 2011, Nature, 479, 372

Langer, N. 1991, Astronomy and Astrophysics, 252, 669

Langer, N., Fricke, K. J., & Sugimoto, D. 1983, Astronomy and Astrophysics, 126, 207

Lecoanet, D., Schwab, J., Quataert, E., et al. 2016, ApJ, 832, 71

Lesaffre, P., Podsiadlowski, P., & Tout, C. A. 2005, MNRAS, 356, 131

Livio, M., & Mazzali, P. 2018, PhR, 736, 1

Moriya, T. J., Tominaga, N., Langer, N., et al. 2014, A&A, 569, A57

Nomoto, K. 1984, ApJ, 277, 791

Nomoto, K., & Kondo, Y. 1991, ApJL, 367, L19

Nugis, T., & Lamers, H. J. G. L. M. 2000, Astronomy and Astrophysics, 360, 227

Paczyński, B. 1972, Astrophys. Lett., 11, 53

—. 1973, Astrophys. Lett., 15, 147

Paxton, B., Bildsten, L., Dotter, A., et al. 2011, The Astrophysical Journal Supplement Series, 192, 3

Paxton, B., Cantiello, M., Arras, P., et al. 2013, The Astrophysical Journal Supplement Series, 208, 4

Paxton, B., Marchant, P., Schwab, J., et al. 2015, The Astrophysical Journal Supplement Series, 220, 15

Paxton, B., Schwab, J., Bauer, E. B., et al. 2018, The Astrophysical Journal Supplement Series, 234, 34

Paxton, B., Smolec, R., Gautschy, A., et al. 2019, arXiv e-prints, arXiv:1903.01426

Potekhin, A. Y., Chabrier, G., & Rogers, F. J. 2009, Phys. Rev. E, 79, 016411

Schwab, J., Bildsten, L., & Quataert, E. 2017, MNRAS, 472, 3390

Schwab, J., & Garaud, P. 2019, ApJ, 876, 10

Schwab, J., Quataert, E., & Bildsten, L. 2015, Monthly Notices of the Royal Astronomical Society, 453, 1910

Schwab, J., & Rocha, K. A. 2019, The Astrophysical Journal, 872, 131

Siess, L. 2006, A&A, 448, 717

—. 2009, A&A, 497, 463

Stein, J., Barkat, Z., & Wheeler, J. C. 1999, ApJ, 523, 381

Suzuki, T., Toki, H., & Nomoto, K. 2016, The Astrophysical Journal, 817, 163

Tauris, T. M., Langer, N., Moriya, T. J., et al. 2013, ApJ, 778, L23

Tauris, T. M., Langer, N., & Podsiadlowski, P. 2015, MNRAS, 451, 2123

Timmes, F. X., Woosley, S. E., & Taam, R. E. 1994, ApJ, 420, 348

Tsuruta, S., & Cameron, A. 1970, Astrophysics and Space Science, 7, 374

Waldman, R., & Barkat, Z. 2007, The Astrophysical Journal, 665, 1235

Wang, B. 2018, Research in Astronomy and Astrophysics, 18, 049

Wang, B., & Han, Z. 2012, New Astronomy Reviews, 56, 122

Woosley, S. E., Wunsch, S., & Kuhlen, M. 2004, ApJ, 607, 921

Zha, S., Leung, S.-C., Suzuki, T., & Nomoto, K. 2019, arXiv e-prints, arXiv:1907.04184